Supplementary Information:
Advancing the Self-Assembly of Binary Colloidal Crystals of Tetrahedra and Octahedra with Confinement

Nathan C. Huang,[a] Rachael S. Skye,[a] and Julia Dshemuchadse[a]*

[a] *Department of Materials Science and Engineering, Cornell University, Ithaca, NY 14853, USA. E-mail: jd732@cornell.edu*

S1 Local motifs at different packing fractions

In an ideal, stoichiometric binary crystal, each octahedron is surrounded by 8 tetrahedra, and each tetrahedron is surrounded by 4 octahedra. Radial distribution functions (RDFs) of all types of neighbor pairs are shown in Fig. S1: motifs of tetrahedra–tetrahedra, octahedra–octahedra (both corresponding to defects), and tetrahedra–octahedra (corresponding to the ideal bulk structure). Integrating these RDFs allows the quantification of the frequency of each of these neighbor pairs, as shown in Fig. S2.

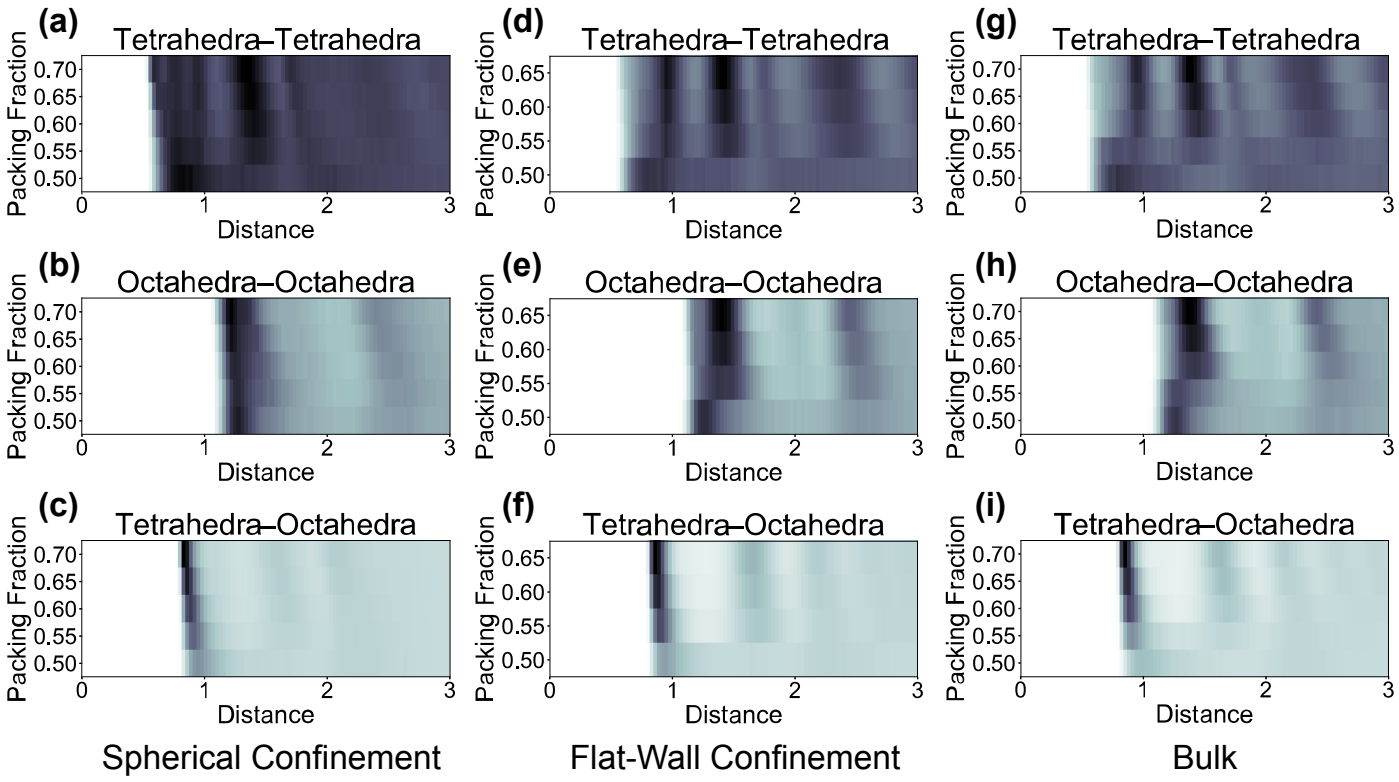

Fig. S1 Typewise radial distribution functions (a–c) in spherical confinement, (d–f) in flat-wall confinement, and (g–i) in bulk simulations. RDFs are computed for (a, d, g) only tetrahedra, (b, e, h) only octahedra, and (c, f, i) tetrahedra–octahedra pairs.

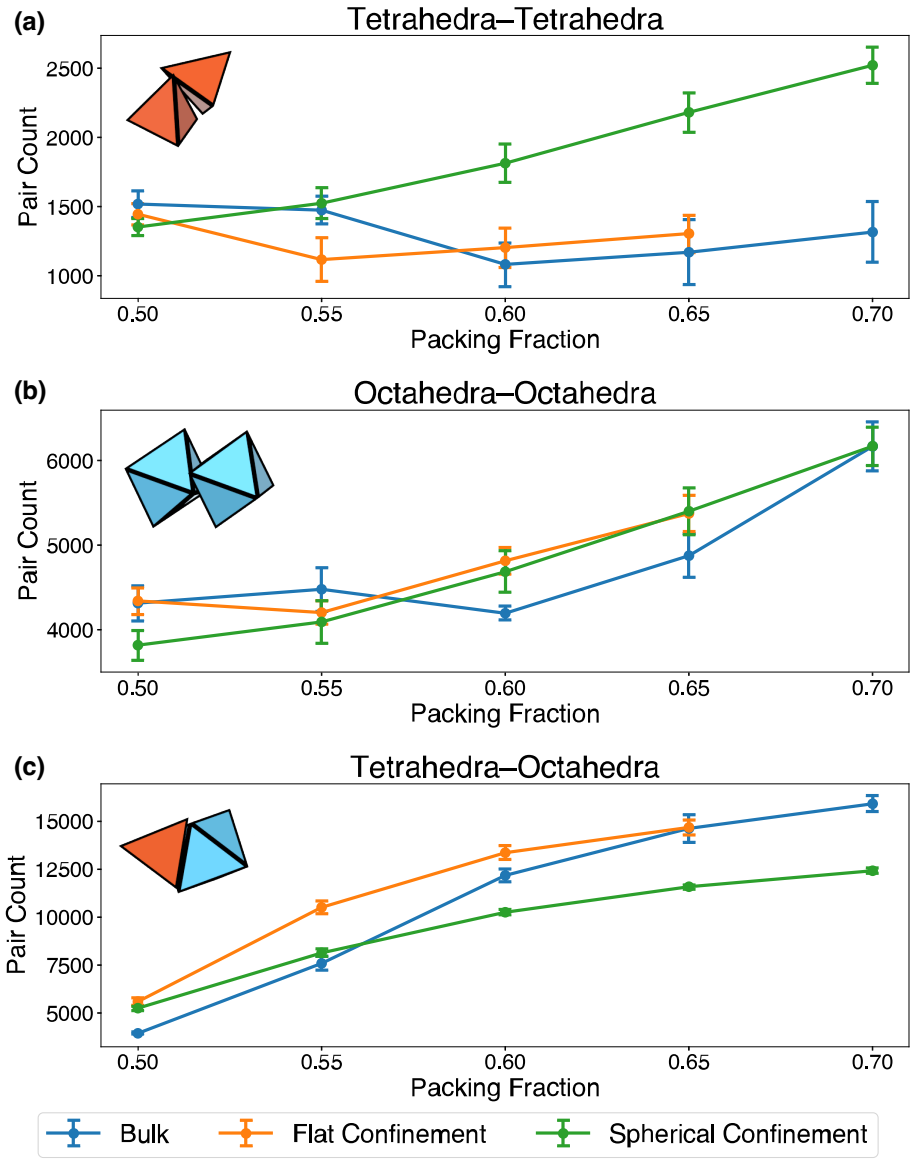

Fig. S2 Local motifs of adjacent tetrahedra–tetrahedra, octahedra–octahedra, and tetrahedra–octahedra pairs *(top to bottom)*, with varying packing fraction at stoichiometry 65% tetrahedra and 35% octahedra. (a) Tetrahedra–tetrahedra neighbor pairs and (b) octahedra–octahedra neighbor pairs correspond to defect motifs, while (c) tetrahedra–octahedra pairs correspond to the defect-free bulk structure. Simulations of the system in bulk, in flat-wall confinement, and in spherical confinement are displayed in blue, orange, and green color, respectively. Particle motifs were quantified for systems containing $N = 4096$ particles each.

S2 Local motifs at different stoichiometries

To investigate the impact of confinement on systems with non-ideal stochiometries, the self-assembly of systems with excess tetrahedra or octahedra is simulated. Fig. S3 shows the RDFs of systems containing 50% to 80% tetrahedra. When one component is in excess, its single-component phase forms in the system, as evidenced by the peaks between $r = 0.5$ to 0.75 when tetrahedra are in excess and between $r = 1.15$ to 1.4 when octahedra are in excess. These peaks narrow and become less intense in flat-wall confinement compared to bulk simulations. This indicates that the single-component phases form in lower relative quantities when one component is in excess, resulting in crystals with lower defect concentrations. This effect is observed at both low ($\phi = 0.55$) and higher ($\phi = 0.65$) packing fractions.

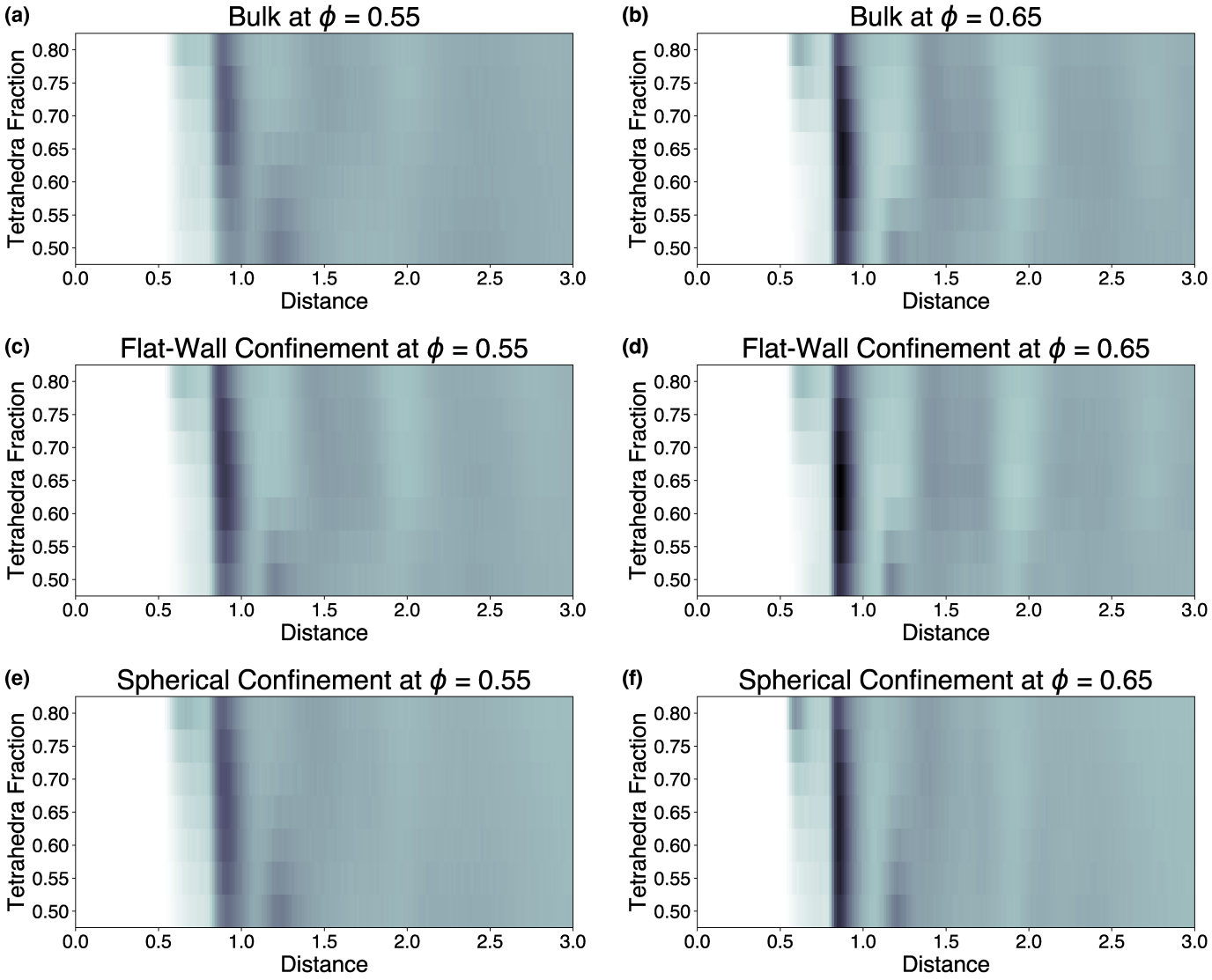

Fig. S3 Radial distribution functions of tetrahedra and octahedra in bulk at (a) $\phi = 0.55$ and (b) $\phi = 0.65$, in flat-wall confinement at (c) $\phi = 0.55$ and (d) $\phi = 0.65$, and in spherical confinement at (e) $\phi = 0.55$ and (f) $\phi = 0.65$. Simulated systems contain $N = 4096$ particles. RDFs are scaled linearly with the relative density of particles and normalized to the highest density within each type of system.

Quantifying the relative occurrence of tetrahedra–tetrahedra, octahedra–octahedra, and tetrahedra–octahedra pairs gives an indication of the relative occurrence of the ideal crystal compared to single-phase defects. Fig. S4 shows the pair counts at different stoichiometries, demonstrating that, as the fraction of tetrahedra increases, the relative fraction of the single-component tetrahedra phase increases (Fig. S4a) and the single-component octahedra phase decreases (Fig. S4b). Fig. S4c shows that systems in flat-wall confinement have the highest proportion of ideal tetrahedra–octahedra pairs. In contrast, systems in spherical confinement have higher proportions of ideal pairs than the bulk at low tetrahedra fraction, but at high tetrahedra fraction the difference between spherical confinement and the bulk crystal is small.

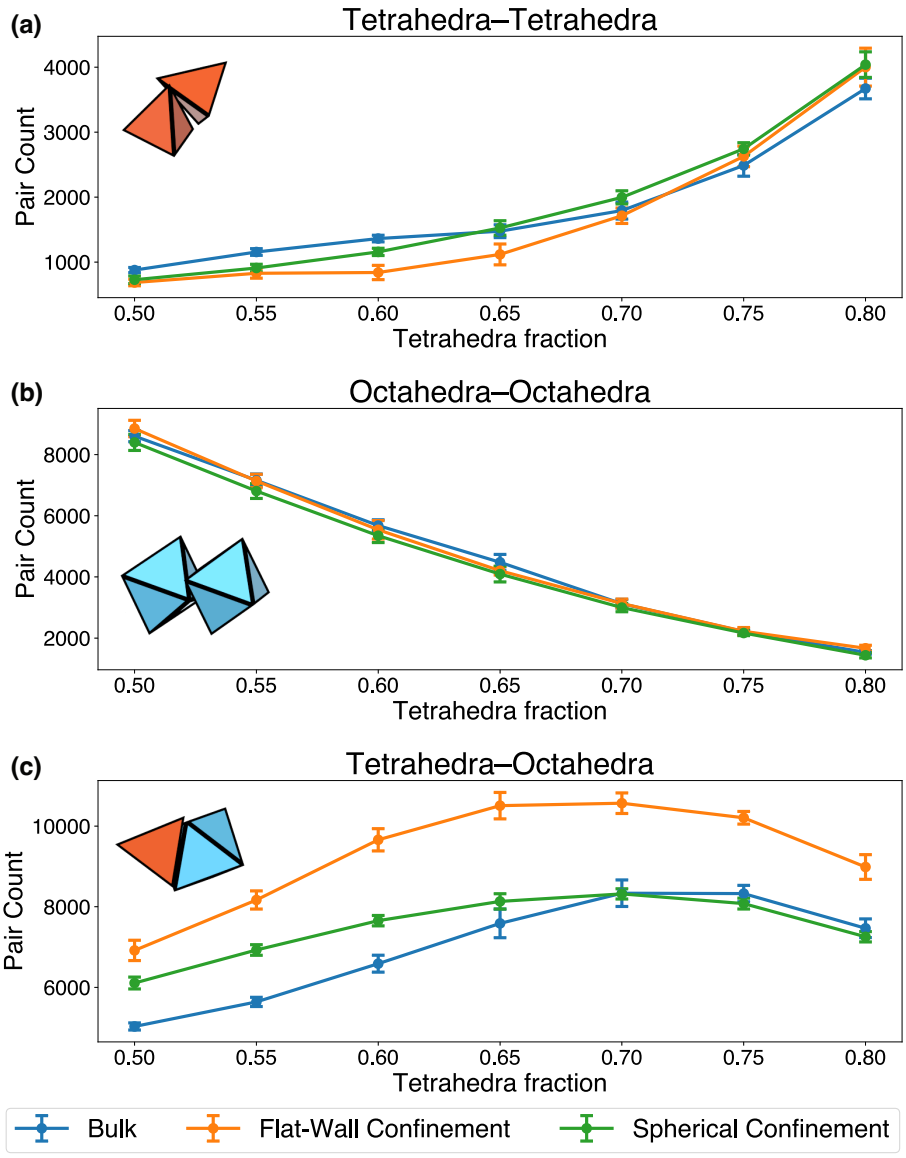

Fig. S4 Relative probabilities of (a) single-component tetrahedra, (b) single-component octahedra, and (c) the binary crystal phases forming in bulk, in flat-wall, and in spherical confinement at compositions between 50% and 80% tetrahedra and at packing fraction $\phi = 0.65$.

S3 Crystallization Process

Defined layers develop in confined systems, from the confining wall inward. These layers begin to develop before crystallization, as quantified in Fig. S5 and visualized in Fig. S6. By following a simulation through compression, we observe that crystallization begins near the walls and that layers rapidly develop inwards. Note that in a spherical container, the total number of particles in the center of the container is small, causing the distribution function to be washed out; the center does not exhibit a layered structure.

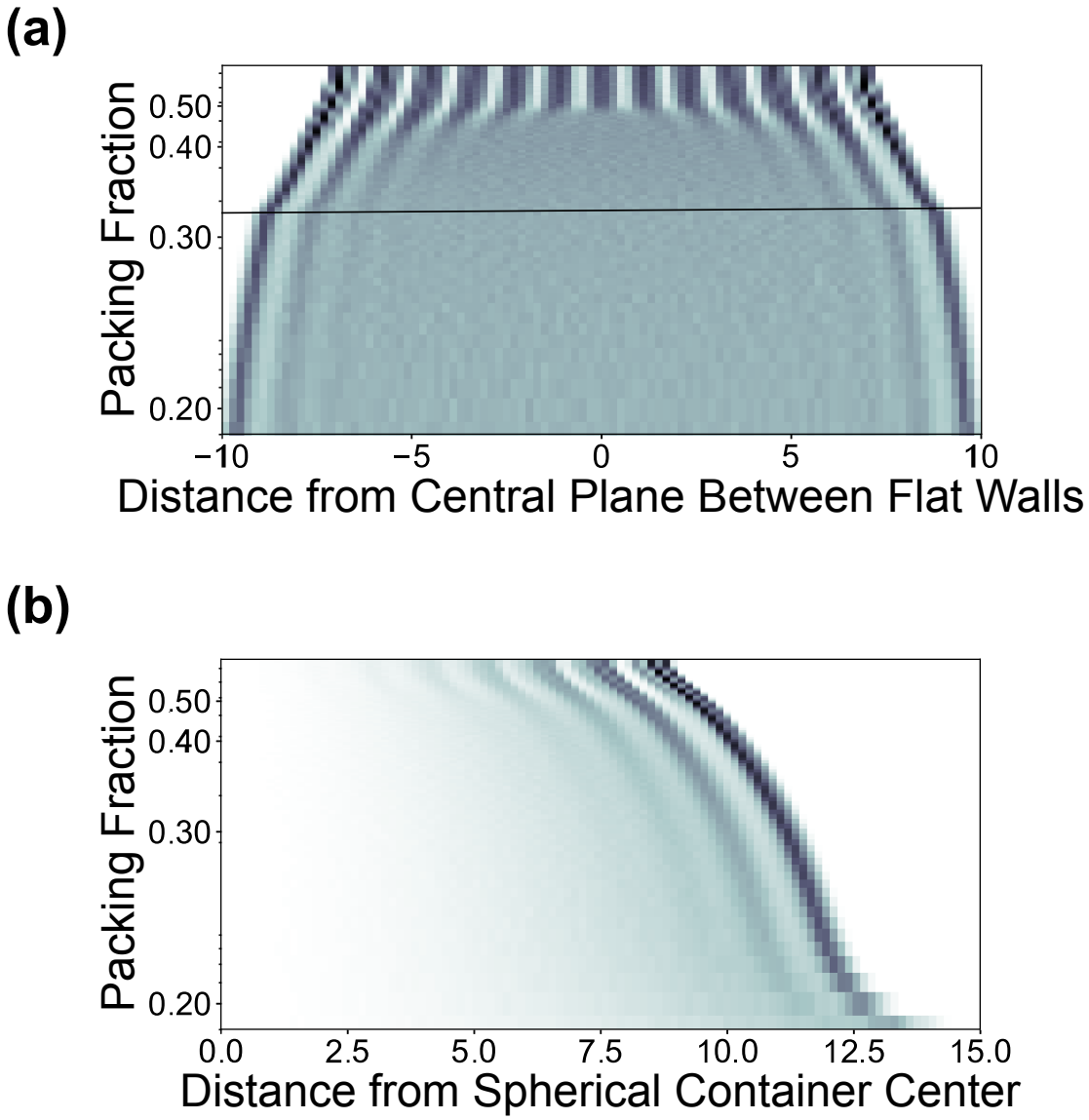

Fig. S5 Distribution of particles (a) in flat-wall confinement, perpendicular to the walls, and (b) in spherical confinement, as a function of distance from the container center, showing the development as packing fraction is increased over the course of a simulation. In flat-wall confinement, simulation box aspect ratio and shear moves are started after an intermediate density is reached, marked on the plot with a horizontal line. Packing fraction is plotted on a logarithmic scale, due to the exponential compression scheme employed. The depicted systems had a final packing fraction of $\phi = 0.65$. Color is scaled linearly with the relative number of particles within each type of system, normalized to the highest count.

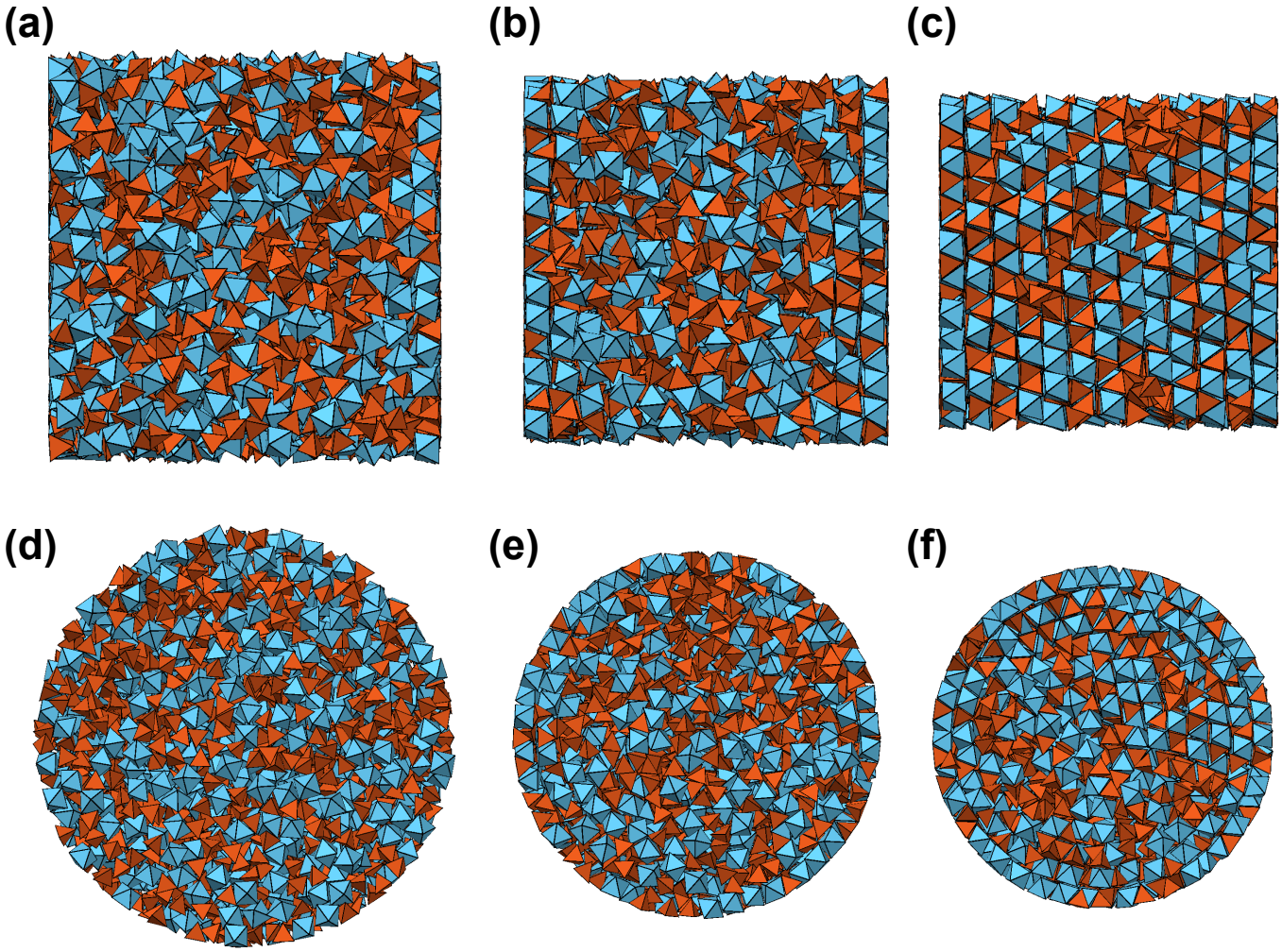

Fig. S6 Representative snapshots of cross-sections through the interior of systems (a–c) in flat-wall confinement and (d–f) in spherical confinement, showing the development of layered structures at early (a,d), intermediate (b,e), and late (c,f) points during the self-assembly simulation. These systems contain 4096 particles have a final packing fraction of $\phi = 0.65$.

S4 Self-assembly behavior in spherical confinement

The structure of the shells formed in spherical confinement can be further investigated *via* the coordination of tetrahedra and octahedra. In spherical confinement, the tetrahedra–octahedra binary crystal develops in defined layers parallel to the wall. These layers are not interdigitated, and thus they can freely rotate with respect to one another. Each layer has non-zero curvature which prevents formation of the ideal crystal, in which the layers would be flat.

To quantify the local environment within a shell, the partial coordination of polyhedra can be determined by isolating the particles that constitute a shell, separated out based on the distance from the confining wall. At least three well-formed shells are observed (see Fig. 6 of the main paper). (In Fig. S7, the layer closest to the confining wall is designated as "shell 1", counting upwards from the wall to the container center.)

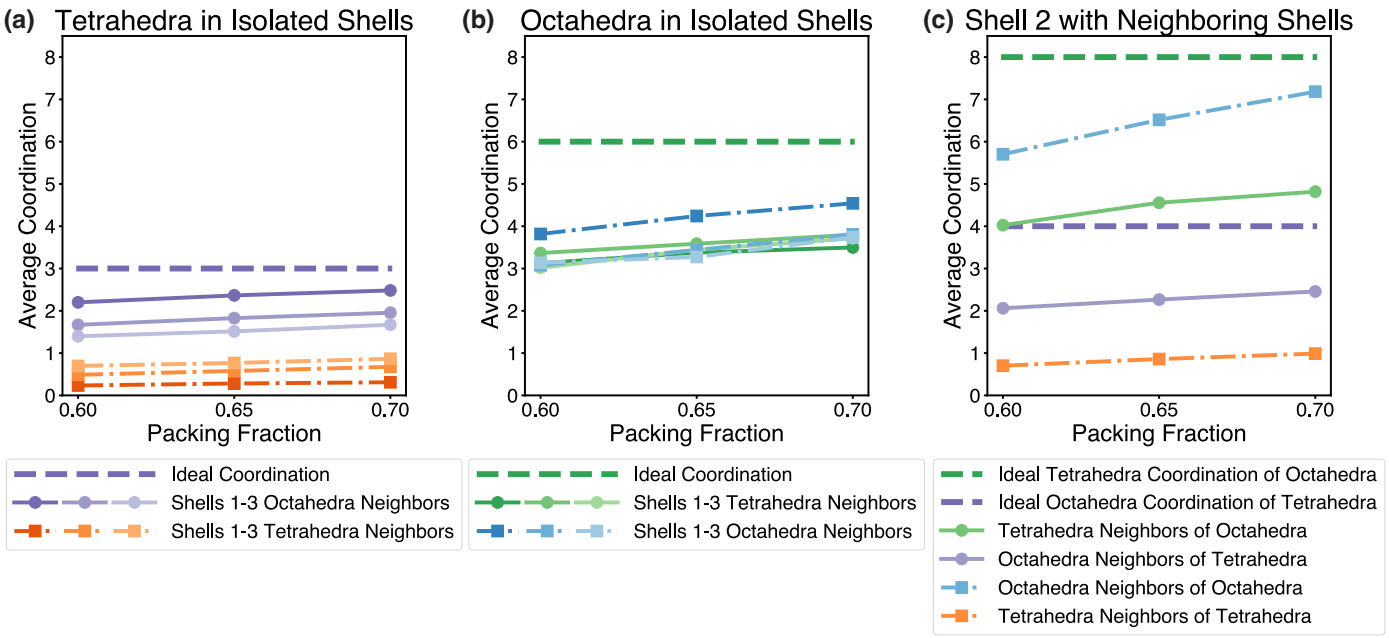

Fig. S7 Ideal *vs.* observed average coordination of (a) tetrahedra and (b) octahedra within shells 1 through 3 (where shell 1 corresponds to the layer closest to the confining wall, and shells 2 and 3 are located increasingly closer to the container center). (c) Ideal *vs.* observed full coordination of polyhedra in the second shell.

In the ideal binary crystal, tetrahedra are coordinated by three octahedra and octahedra are coordinated by six tetrahedra within each layer. Tetrahedra in the outermost shell are almost ideally coordinated, with very few tetrahedron–tetrahedron neighbor defects (see Fig. S7a). As shells form closer to the center of the container, tetrahedra have a decreasing number of neighbors that are octahedra and an increasing number of neighbors that are tetrahedra. This suggests that single-component tetrahedra defects are more common in the inner shells, perhaps induced by the increasing curvature that makes it more difficult for the binary crystal to form.

On the other hand, large amounts of octahedron–octahedron neighbor defects are present in all three shells (see Fig. S7b). This reflects the scarring observed in the crystals formed in spherical confinement, which is dominated by octahedra (see below). As shells form closer to the center of the container, fewer octahedron–octahedron neighbor defects are observed. The opposite trends observed for tetrahedron–tetrahedron *vs.* octahedron–octahedron neighbor defects suggests that tetrahedra are pushed towards the center of the container, where they then form single-component defects, while octahedra are pushed toward the container wall.

However, when considering the full coordination of the second shell from the wall (shell 2), the average full coordination of the full binary crystal structure falls far short of the ideal coordination (see Fig. S7c). The full coordination in the ideal binary crystal consists of four octahedra around a tetrahedron and eight tetrahedra around an octahedron. However, for these neighbor pairs the average coordination in the second shell only increases by around half a particle from their partial coordination within the shell, and we observe a much higher prevalence of octahedron–octahedron defect particle pairs. The high *intra–shell* order but low *inter–shell* order suggests that shells have little interaction with each other, presumably

resulting from the ability for each shell to independently rotate. This observation is in line with the fact that each distinct layer coincides with a flat shear plane in the ideal binary crystal: there is no interpenetration between shells that would prevent free rotation, and the differing curvature of subsequent layers results in the shells being incommensurate with respect to each other.

S5 Scarring in Spherical Confinement

Due to the finite curvature of a spherical container, a crystal growing in this confinement geometry must be defective. These systems will often form defects in otherwise well-ordered layers—effectively "scars"—which are topologically required in order to form a crystal structure composed of flat layers, while conforming to a curved surface. In the binary system, surface scars are dominated by single-phase clusters of octahedra, as shown in Fig. S8.

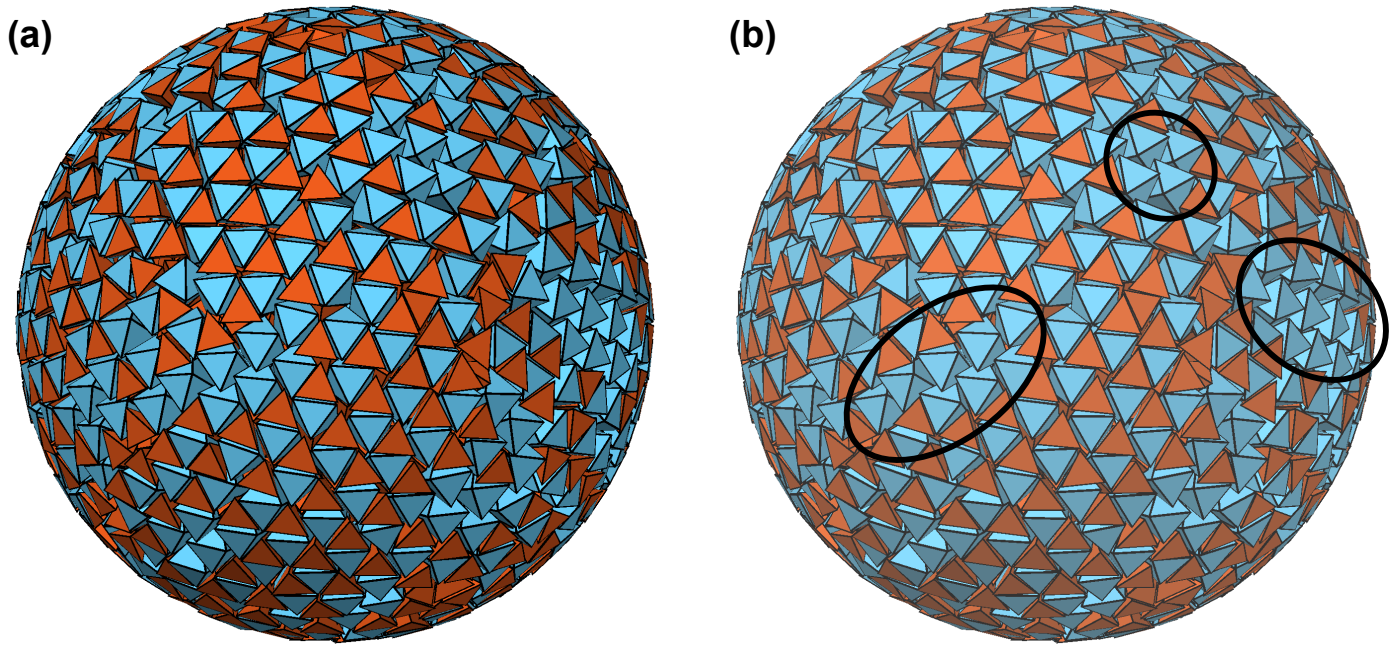

Fig. S8 A representative simulation of a near-stoichiometric system of 65% tetrahedra–35% octahedra in spherical confinement, showing the surface defects dominated by octahedral particles, showing a the container exterior and b the same view with sample defects highlighted.